ADVANCED MATERIALS
www.advmat.de

Anomalous-Chern Steering of Topological Nonreciprocal Guided Waves

*Haoye Qin, Zhe Zhang, Qiaolu Chen, Zhechen Zhang, and Romain Fleury**

Nonreciprocal topological edge states based on external magnetic bias have been regarded as the last resort for genuine unidirectional wave transport, showing superior robustness over topological states with preserved time-reversal symmetry. However, fast and efficient reconfigurability of their trajectory has remained a formidable challenge due to the difficulty in controlling the spatial distribution of magnetic fields over large areas and short times. Here, this persistent issue is solved by leveraging the rich topology of unitary scattering networks, and achieve fast steering of nonreciprocal topological transport at an interface between a Chern and an anomalous topological insulator, without having to control a magnetic field. Such interface can be drawn by doping the network with scatterers located at the center of each link, whose level of reflection is electrically tuned. With experiments in the GHz range, the possibility to actively steer the way of unidirectional edge states is demonstrated, switching the transmission path thousands of times per second in a fully-robust topological heterostructure. The approach represents a significant step towards the realization of practical reconfigurable topological meta-devices with broken time-reversal symmetry, and their application to future robust communication technologies.

1. Introduction

Topological edge states, which correspond to the propagation of waves along the boundaries of insulators with distinct bulk topology, have been the subject of extensive research due to their high potential for enabling point-to-point transport with increased control and robustness. They can be obtained from various topological phases, including valley insulators,[1–3] Weyl semimetals,[4–7] symmetry-protected phases,[8–10] Chern insulators,[11,12] or Floquet systems.[13,14] These states originate from a global property of the bulk, associated to a topological invariant, which cannot disappear unless the entire system goes through large deformations or symmetry changes.[15,16] Therefore, they can exhibit partial or complete resilience against local imperfections or distributed disorder, which makes them ideal candidates as information and energy carriers in electronics, photonics, and communication technologies.

On the other hand, the idea of reconfigurability is thriving in various systems like antennas,[17] nanostructures,[18] metasurfaces,[19] 5-6G communications,[20] and networks,[21] seeking tunability and adaptability to overcome the limitations of fixed-function devices. Although adaptable wave functionalities can be easily controlled by external stimuli, changes along a wave's path are inherently associated with impedance fluctuations inducing back-reflections, and large reconfiguration is typically associated with a loss of efficiency. To try and mitigate this problem, significant efforts have been dedicated to develop reconfigurable topological systems, in which reconfiguration would benefit from a certain level of topological protection, ideally preventing entirely any form of backscattering and easing the addition of new functionalities on the wave path.[22–30] The usual mechanism relies on reconfiguring the position of a topological interface, aka domain wall, formed at the boundary between two topologically distinct bulk insulators,[25] thereby modifying the edge state path. To work with non-reciprocal edge states would require to control dynamically and over large areas the external magnetic fields responsible for strong topological protection. The required control circuitry would arguably be impractical, bulky, and inefficient. Accordingly, prior arts have restricted themselves to time-reversal invariant systems that do not break reciprocity,[31–33] which at most provide resilience to particular, weak perturbations. In addition, previous works focused mostly on slow, mechanical reconfigurability, which does not cater to the needs of reconfigurable systems and their applications.

Here, we conceive, design, and experimentally demonstrate a fully robust, reconfigurable topological system capable of steering a nonreciprocal edge state along different trajectories, and changing its status at will several thousands of times per second. The idea is based on the unique physics of unitary topological systems,[34–36] which are non-reciprocal topological insulators that support not only the Chern phase, but also a distinct, extremely robust anomalous phase.[37,38] Crucially,

H. Qin, Z. Zhang, Q. Chen, Z. Zhang, R. Fleury
Laboratory of Wave Engineering
School of Electrical Engineering
École Polytechnique Fédérale de Lausanne (EPFL)
Lausanne 1015, Switzerland
E-mail: romain.fleury@epfl.ch

The ORCID identification number(s) for the author(s) of this article can be found under https://doi.org/10.1002/adma.202401716

DOI: 10.1002/adma.202401716

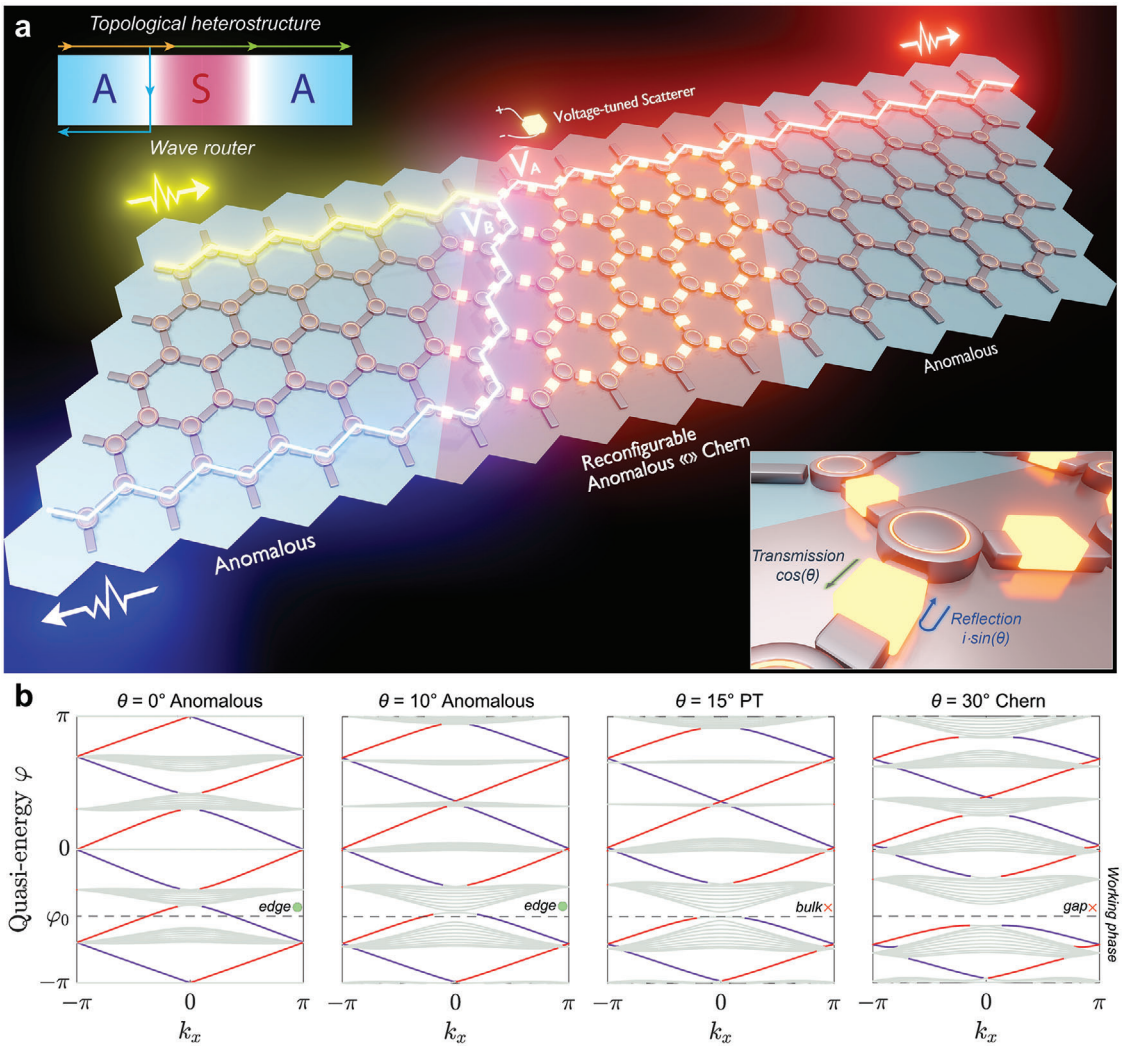

Figure 1. Anomalous-Chern steering of nonreciprocal edge states in a topological heterostructure. a) Topological heterostructure, in which two anomalous insulators (represented by *A*, top inset) surround a middle region whose gap size and topology is electrically reconfigurable (represented by *S*). Region *A* is a honeycomb network of circulators connected by transmission lines (TLs) of phase delay φ. Region *S* is similar to region *A*, except for the introduction of unitary scatterers at the middle of each TL (bottom inset, yellow boxes). The scattering amplitude of the scatterers is controlled by the parameter θ and proportional to an external DC voltage. This allows to reconfigure the topological phase of the region *S* from anomalous to Chern. When the region *S* is in anomalous phase, a wave input from the left (yellow arrow, V_A) will tend to flow undisturbed along the edge, following the red signal path. In contrast, when S is switched to the Chern phase, the input meets an anomalous-Chern topological interface, and must go down the blue signal (V_B).b) Band structure of the *S* region at different values of the scattering strength θ from an anomalous phase ($\theta < \theta_c$) to a Chern phase ($\theta > \theta_c$). The phase transition (PT) occurs at $\theta_c = 15°$. The working phase φ_0 of the topological heterostructure is highlighted by a dashed line. Modes localized to the top and bottom are shown in red and blue, respectively. The corresponding gap invariant W_ψ and Chern number for bands from top to bottom are 1,1,1,1,1,1 and 0,0,0,0,0,0 for $\theta = 0°$ and 10°, PT for $\theta = 15°$, 1,1,1,1,0,1 and 0,0,0,0,-1,1 for $\theta = 30°$.

the anomalous-Chern topological interface does not require a change in the magnetic field, but only a reflection contrast, which allows us to reconfigure it electrically by doping the network with simple variable capacitors. We design a topological anomalous-Chern heterostructure that can be gradually constructed or destroyed, effectively sending the signal to different ports in a unidirectional, back-scattering immune way, with a fully reversible manner. The strongly robust topological nature of the anomalous-Chern interface is theoretically and experimentally evidenced by implementing various defects in the shape and composition of the reconfigurable heterostructure.

2. Results

As an example, we achieve topological steering of nonreciprocal edge states in a topological heterostructure, schematically represented in the top left corner of **Figure 1**a. It is composed of a topological insulating heterostructure involving two static domains operated in the anomalous phase (*A*), surrounding a third one (*S*). Region *S* is similar to region *A*, except for the introduction of unitary scatterers at the middle of each transmission line (TL). Geometrically analogous to a FET transistor, this electrically reconfigurable active domain *S* plays the role of a depletion region

by allowing full control over the insulating gap size, whose underlying topology can be switched between the anomalous and Chern (*C*) phases. The center of Figure 1a depicts an implementation of this concept using a honeycomb network made of circulators, positioned at the corners of a hexagonal lattice, and connected by transmission lines of phase delay φ, which corresponds to the quasi-energy of the underlying unitary Bloch eigenproblem (see Experimental Section). Each microwave circulator is realized by an azimuthally-symmetric ferrite cavity (e.g., made of yttrium iron garnet) biased by a permanent magnet, thereby breaking reciprocity. The magnetic bias induces a proportional frequency splitting between the two originally-degenerated counter-propagating eigenmodes, in analogy to the Zeeman effect. In absence of this magnetic bias, the two eigenmodes have the same frequency $\omega_+ = \omega_-$. In the presence of a non-zero magnetic bias, the two eigenmodes exhibit a non-zero frequency splitting of $\Delta\omega = |\omega_- - \omega_+| > 0$. This feature has been widely employed to realize strong nonreciprocity in microwave circulators or isolators,[39–42] and for our case, coupled mode theory can be unitized to fully model the nonreciprocal scattering phenomenon, including its frequency dispersion (see Supporting Information). In such networks, the reflection level of individual circulators controls the topology of the network: at low enough reflection, it finds itself in an anomalous phase, whereas increasing the reflection closes the bandgap and reopens it in a Chern phase (see Experimental Section and Ref. [37]). Therefore, we propose to start from low-reflection circulators (i.e., an anomalous phase) and construct the depletion region *S* by doping it with additional reciprocal scatterers (yellow blocks) placed at the center of the TLs (see Experimental Section for the scatterer's impact on Bloch eigenproblem). These unitary scatterers effectively increase the level of reflection for waves traveling within the depletion region. In practice, their reflection ($i\sin(\theta)$) and transmission ($\cos(\theta)$) will be tuned by an external voltage.

The effect of increasing the doping on the band structure of the depletion region is illustrated in Figure 1b. When $\theta = 0$, the band structure is the one of a typical anomalous topological insulator, exhibiting separated bulk bands (6 in total including two flat bands, in grey), with edge states in every bandgap, propagating either at the top (red lines) or bottom (purple lines). The Chern numbers of all bands are zero. This behavior is still valid for low enough scattering strength (e.g., $\theta = 10°$), although the sizes of the gaps are modified. In particular, the gap around the working phase $\varphi_0 = -\pi/2$ starts closing. At $\theta = \theta_c = 15°$, this band gap closes, triggering a phase transition to a Chern phase with a single trivial bandgap around φ_0 (see plot at $\theta = 30°$). As a side note, past the PT point, edge-like modes occur near the dashed line but without connecting the two bulk bands, eventually fully detaching from them, which implies a trivial nature.

To leverage this effect, we now choose to operate at φ_0. This simple design choice can be made by tuning properly the length of the network links at the frequency of interest. We expect that for small enough values of the scattering strength $\theta < \theta_c$, the reconfigurable region operates in an anomalous phase ($S = A$), and provides an edge state that makes it possible for an input signal incident from the left (in yellow) to be transmitted to the right (red signal path). This *AAA* configuration corresponds to the "on" state of the heterostructure, which operates with an open gate. Conversely, at high enough values of the scattering strength $\theta > \theta_c$, the input wave meets a topological interface at the entrance of the depletion region and must travel down until it reaches the bottom edge of the input region, escaping at the bottom left (blue signal path). This *ACA* configuration corresponds to "off" operation with a closed gate. Close to θ_c, a transition will occur in which part of the power will be able to go through (by evanescent tunneling), while the other part would be reflected down the blue signal path. This behavior can be classified as a topological router that splits the charge current into two parts, with a tunable allocation ratio.

Figure 2a evidences this behavior as a topological router with numerical simulations. Note that the thickness of the depletion region has been tuned such that at the transition, the power is split equally to ports 2 and 3, although other allocation ratios are possible. The full picture is provided in Figure 2b, which plots the evolution of transmitted power at port 2 (P_2) and port 3 (P_3) when increasing the scattering strength, confirming the gradual switching capability of the topological heterostructure. Figure 2c plots the corresponding isolation ratio which can take values from –40 to +40dB. This dynamic range is controlled by the depth of the depletion layer. For the interested reader, extra studies are reported in the Supporting Information, including the possibility to operate with interfaces of irregular shapes and irregular doping. The case of topological combiner operation is also possible and reported (see Supporting Information).

Remarkably, the steering capability of Chern-anomalous interfaces comes with extreme robustness to various practically relevant parameters, including global disorder in the value of the phases provided by each network link, or imperfections in the doping scheme. In **Figure 3a**, we impart a maximum phase disorder, randomly distributed in $[0, 2\pi]$, to every TL in the network, and study the operation of the topological heterostructure under these extreme conditions by varying the doping strength $\theta = 0° - 80°$. In the bottom plot, we conduct a statistical analysis over 200 random realizations of phase disorder, and evaluate the averaged transmissions to ports 2 and 3 (solid lines), as well as their first and last quartiles Q1 and Q3 (dashed lines). We find that the topological heterostructure is still working exceptionally well, with most realizations closely following an average behavior similar to the one of the clean limit. Field maps at randomly selected realizations of disorder confirm that wave propagation is altered by the disorder, but not the resulting transmission to the output ports. Yet, another form of disorder generally occurs in such active reconfigurable systems. Unwanted disconnection to the control signal is quite common, and may induce on/off scattering strength (θ) disorder. In Figure 3b, we consider a situation in which a quarter of the scatterers of the reconfigurable region are disconnected (so that their scattering strength is fixed to $\theta = 0°$). It is noteworthy and expected that the critical value of θ for achieving power switch becomes larger than clean limit under the presence of disorders, mainly due to reduced efficiency of the doped scatterers. This is also in line with the results with tilted interfaces, where the power switch point sufficiently moves to larger value with smaller number of doped scatterers (see Figure S6, Supporting Information). Again, our statistical studies show that the operation of the topological heterostructure as a power switch remains remarkably robust.

We now experimentally demonstrate dynamical steering of nonreciprocal edge states for microwaves in the C band, by

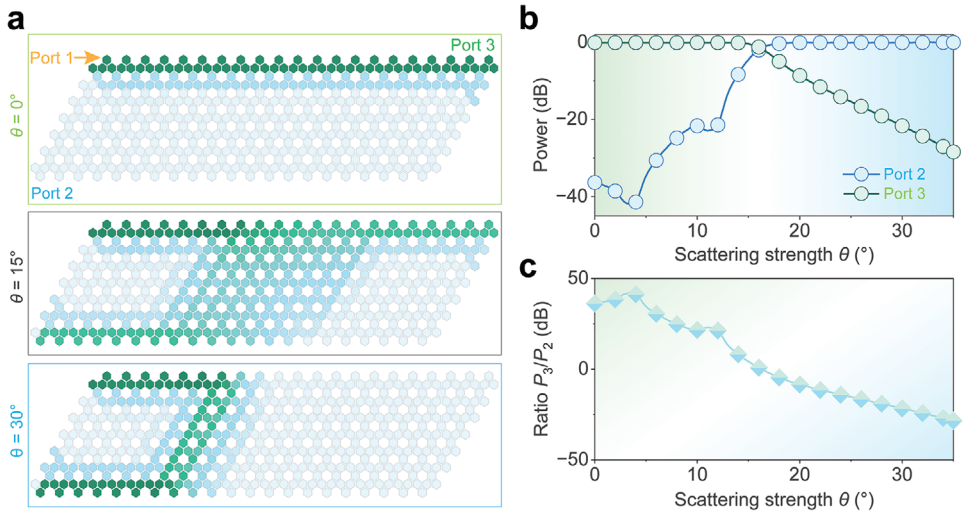

Figure 2. Numerical simulations of non-reciprocal power steering in a topological heterostructure. a) Simulated field amplitude maps excited by a wave input at port 1, for different values of the scattering strength, namely $\theta = 0°$, 15°, and 30°. At $\theta = 0°$ (top, *S* is in anomalous phase), the input wave travels undisturbed along the top boundary, and is unidirectionally transmitted to port 3, with zero transmission to port 2. Conversely, at $\theta = 30°$ (bottom, *S* is in Chern phase), the nonreciprocal wave is steered to port 2 along the anomalous-Chern interface, with vanishing transmission to port 3. Near the transition (middle panel), an intermediate behavior with coupling into bulk is observed, due to partial wave transmission through the middle region. b) Power transmission at ports 2 (P_2) and 3 (P_3) versus θ, and c) corresponding ratio P_3/P_2. Increasing θ continuously in the region *S* changes the wave destination from port 2 to port 3, reconfiguring the chiral wave path.

building the topological heterostructure shown in **Figure 4**. The printed circuit board hosts 36 ferrite circulators that are connected through microstrip lines, and three input/output ports are implemented via welded SMA connectors (Figure 4a). The reconfigurable region is highlighted by a dashed box. The voltage-tunable scatterers added to the transmission lines are implemented by three near-field coupled split ring resonators, the middle one being frequency shifted by a varactor, whose capacitance is controlled by an external static voltage (DC bias). By increasing the DC bias from 0 to 30 V, the capacitance of the varactor will decrease from 2.5 to 0.6 pF, which switches the initially high transmission of the coupled split rings to a low value, generating higher reflection. In other words, the scattering strength θ and the applied DC bias have a monotonic relationship (see Supporting Information). The proper operation of the topological heterostructure is evidenced in Figure 4b at 5.5 GHz. By tuning the scattering strength from 0° to 66° (corresponding voltage from 0 to 30 V), we measure the output power at ports 2 and 3, and observe a clear switching between them, consistent with the predictions of Figure 2. The corresponding power ratio P_3/P_2 is plotted in Figure 4c, showing a gradual change from the "on" to the "off" state. Figure 4d reports the measured field amplitude distribution in the heterostructure network at the scattering strengths of $\theta = 0°$, 45°, and 66°, which confirm that the operation of the device as a switch is indeed mediated by the nonreciprocal topological edge states, as anticipated by our previous simulations. Different tilted interfaces were also tested with good steering consistency (see Supporting Information). We now turn to an experimental validation of the robustness of the topological heterostructure to on/off scattering strength disorder. The other type of disorder, global phase disorder, has already been experimentally investigated elsewhere.[37,38] Thus, we randomly select 5 out of the 16 varactors in the active region and disconnect them. Figure 4e illustrates this particular random disconnection, and plots the heterostructure output powers as a function of the scattering strength of the varactors that are still connected. The evolution closely follows the prediction of Figure 4b and maintains the functionality of the system as a power switch even under such drastic flaws in the control scheme, confirming that the remarkable resilience of the topological heterostructure is a clear observable in real-life scenarios.

Finally, we come back to one of our original motivations and demonstrate the possibility to dynamically steer non-reciprocal edge states by the experiment of Figure 4f. We introduce a square wave modulation of 30 V and 250 Hz to the bias voltage of the reconfigurable region *S*, and observe the effect on the output power ratio of the topological router. Our measurement reveals that the system is capable to switch rapidly, re-routing the power sequentially between port 2 and port 3. We estimated the rise time of the output amplitude to be 0.33 ms, corresponding to a maximum switching frequency of 3 kHz. Such a speed is more than comfortable for communication applications, since it provides sufficient bandwidth for voice transmission, telemetry, control systems, and certain types of wireless communication. It's noteworthy that the upper limit of modulation speed is merely constrained by the transient response of the varactors, and may be significantly improved using alternative tuning components like PIN diodes specialized for high frequency applications. To this end, we note that highly efficient RF switches have been recently demonstrated up to THz frequencies.[43]

3. Conclusion

In conclusion, topological steering of nonreciprocal edge states has been achieved and experimentally demonstrated in a topological heterostructure, drawing upon the rich topological physics

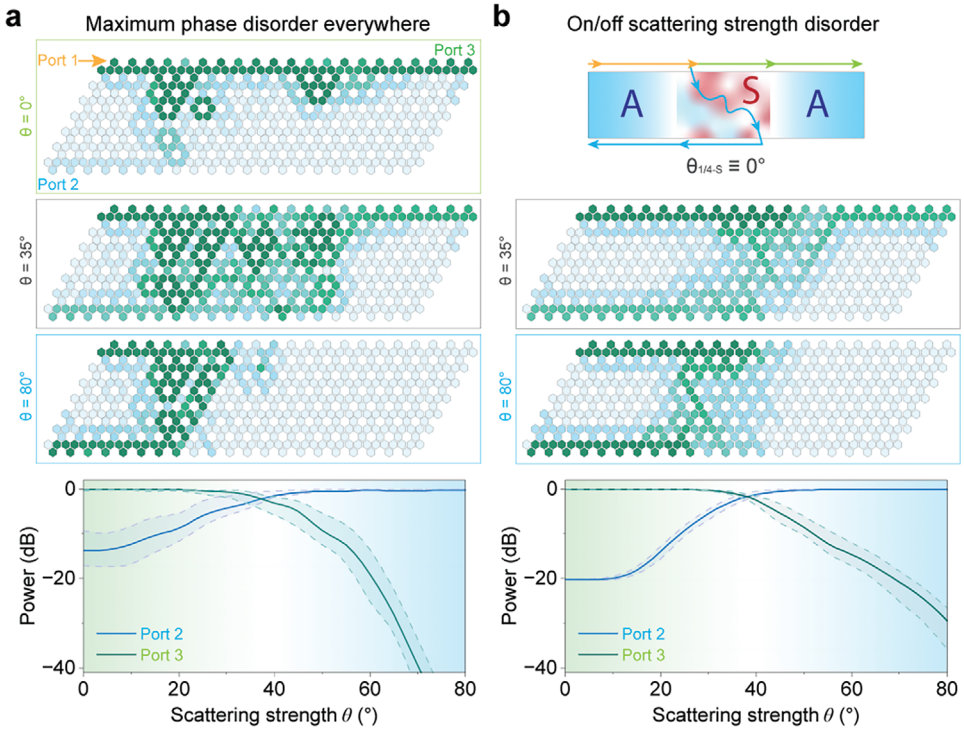

Figure 3. Exceptional topological robustness of anomalous-Chern steering. a) Resilience of topological heterostructures to complete disorder in the link phase delays. We take the topological heterostructure of Figure 2 as the clean-limit case, and randomly shift the values of the phase delays (φ) in the range [0, 2π]. We perform wave transmission statistics over 200 realizations of phase disorder at each value of the scattering strength θ. In the bottom panel, the solid lines represent the average power transmission to port 2 (green) and 3 (blue), while the dashed lines are the first and last quartiles, Q1 and Q3. Three realizations of disorder are shown in the top panels, at $\theta = 0°$, 35°, and 80°, confirming the resilience of the wave paths despite the presence of a high level of distributed phase disorder in the system. b) Robustness of topological heterostructures against on/off scattering strength disorder. Here, for each scattering strength θ, we consider that a randomly selected quarter of the scatterers are disconnected from the external control signal and do not scatter at all ($\theta = 0°$), while the others keep the intended scattering strength value. This situation is schematically illustrated in the inset of (b). By performing a statistic study, we find that also in this case, the functionality of the topological heterostructure is left almost undisturbed. Example of field distributions for two disorder realizations, confirming the robustness of the wave steering process.

of unitary scattering networks, that allow for reconfigurable anomalous-Chern domain walls without having to control a magnetic field. We showed that the topological phase of a heterostructure can be continuously tuned from anomalous to Chern by doping it with voltage-controlled reflectors located within the phase links of the network. Such topological reconfiguration turns the heterostructure into a nonreciprocal router and combiner that behave similarly to PNP- and NPN- electronic transistors, albeit manipulating the electromagnetic power flow instead of the electrical current. The topological robustness of the steering mechanism under extremely disordered conditions was confirmed. This includes perturbations of practical relevance including global phase disorder and faulty varactors with random on/off disconnections. The topological heterostructure can survive considerably large imperfections and irregular interfaces without losing its functionality. Rapid switching of the path of the nonreciprocal edge state was also achieved by modulating the control voltage applied to the depletion region. Our work opens up a new route for rapid and efficient manipulation of nonreciprocal edge states, empowering high-frequency circuits and communication systems with more efficient signal control capabilities, leading to more reliable and efficient data transmission. Switchable chiral electromagnetic flow could lead to the development of more advanced and versatile electromagnetic devices, such as the microwave equivalents of field-programmable gate arrays (FPGAs) or other types of programmable logic devices existing a lower frequencies. Finally, reconfigurable nonreciprocal edge states may enable new possibilities in quantum computing systems,[44,45] in which unidirectional qubit coupling is a much-sought opportunity.

4. Experimental Section

Band Theory of Circulator Networks: This section details i) the derivation of Bloch eigenproblem for band theory, ii) the calculation of topological invariants and classification of unitary scattering network, and iii) the impact of scatterers on band topology.

It is assumed that the circulators exhibit threefold rotational symmetry and that their scattering is unitary, which had been checked by direct measurements. Such scattering matrix was parameterized, noted S_0, in terms of the angles ξ and η, using the form given in Refs. [37,46,47], namely:

$$S_0 = \begin{bmatrix} R & T & D \\ D & R & T \\ T & D & R \end{bmatrix} \quad (1)$$

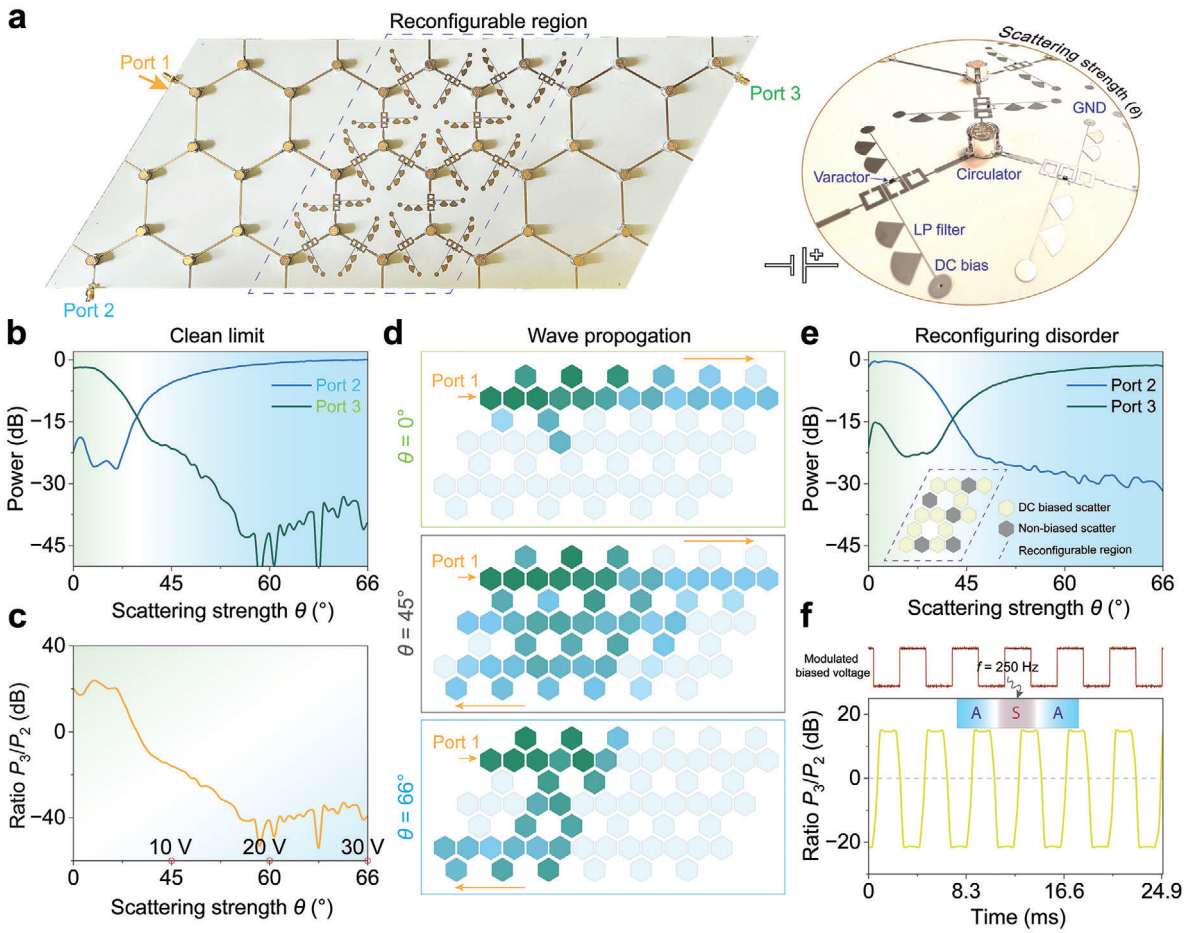

Figure 4. Experimental observation of dynamical anomalous-Chern steering with strong topological robustness. a) Layout of the fabricated topological heterostructure prototype, based on a microwave printed circuit board (PCB) with surface-mount circulators and TLs (left). The reconfigurable region is highlighted by a dashed box. Right: Zoomed-in view of a tunable scatterer implemented with TL-integrated split-ring resonators, a low-pass (LP) filter, and a varactor diode whose capacitance is controlled by a DC bias voltage fed from the other side of the PCB. A one-to-one correspondence exists between the varactor capacitance and the scattering strength θ. b) Measured transmitted power at ports 2 and 3 of the topological heterostructure versus θ, confirming the topological steering of the nonreciprocal edge state. c) The corresponding isolation ratio goes from positive to negative. d) Measured field distribution at every TL at $\theta = 0°$, 45°, and 66° (from top to bottom). The short and long arrows indicate the directions of the input and transmitted power flows. e) Evolution of transmitted power at ports 2 and 3 versus DC bias voltage when randomly disconnecting 5 scatterers from the DC bias. Inset: corresponding disorder realization within S. The faulty scatterers are in grey. f) Dynamic steering experiment, in which the external control voltage is modulated following a 250 Hz square wave with amplitude of 30 V (top inset). The bottom inset shows the time-modulated response of the ratio P_3/P_2, demonstrating the rapid periodic switching of the wave path between the two output ports.

where,

$$R = -1 + \frac{2}{3}\cos\xi e^{i\xi} + \frac{2}{3}\cos\eta e^{i\eta} \tag{2}$$

$$T = \frac{2}{3}\left[e^{-i\frac{2}{3}\pi}\cos\xi e^{i\xi} + e^{i\frac{2}{3}\pi}\cos\eta e^{i\eta}\right] \tag{3}$$

$$D = \frac{2}{3}\left[e^{i\frac{2}{3}\pi}\cos\xi e^{i\xi} + e^{-i\frac{2}{3}\pi}\cos\eta e^{i\eta}\right] \tag{4}$$

here, ξ and η are parameters defined in the range $[-\pi/2, \pi/2]$ with a periodicity of π, and they are respectively related to the deviation of the angular frequency ω from the right-handed (ω_+) and left-handed (ω_-) eigenvalues of the ferrite cavity of the circulator. These non-dimensional parameters emerge naturally in the coupled mode theory of Zeeman-based circulators.[40]

The phase delay band structure was derived in periodic honeycomb scattering networks by considering the two circulators present in a honeycomb unit cell. The action of the scattering matrices on the complex amplitudes of the waves propagating in and out of the circulators was (schematic in Figure S1 of Supporting Information):

$$\begin{bmatrix} a_3 \\ a_1 \\ a_2 \\ a_5 \\ a_6 \\ a_4 \end{bmatrix} = \begin{bmatrix} 0 & S_0 \\ S_0 & 0 \end{bmatrix} \begin{bmatrix} b_1 \\ b_2 \\ b_3 \\ b_4 \\ b_5 \\ b_6 \end{bmatrix} \tag{5}$$

where these vectors concatenate the six complex wave amplitudes incident on the two circulators of the unit cell (noted a_1 to a_6), and the outgoing ones (noted b_1 to b_6). Equation (5) was then multiplied by a unitary

permutation matrix P_0, which exchanges the fifth and sixth rows, the fourth and fifth rows, and the first and second rows, to obtain:

$$|a\rangle = S_{\text{unit cell}}|b\rangle \qquad \text{with} \quad S_{\text{unit cell}} \equiv P_0 \begin{bmatrix} & S_0 \\ S_0 & \end{bmatrix} \tag{6}$$

where $|a\rangle$ and $|b\rangle$ are functions of the position $\boldsymbol{r}$ of the unit cell, with $\boldsymbol{r} = n_1\boldsymbol{\alpha_1} + n_2\boldsymbol{\alpha_2}$, where $\boldsymbol{\alpha_1}$ and $\boldsymbol{\alpha_2}$ are Bravais lattice vectors, and $\boldsymbol{n} = n_1, n_2$ are integers.

With the phase delay lines between circulators, we obtain:

$$b_1(\boldsymbol{r}+\boldsymbol{\alpha_2}) = e^{i\varphi}a_1(\boldsymbol{r}) \tag{7}$$

$$b_2(\boldsymbol{r}+\boldsymbol{\alpha_1}) = e^{i\varphi}a_2(\boldsymbol{r}) \tag{8}$$

$$b_3(\boldsymbol{r}) = e^{i\varphi}a_3(\boldsymbol{r}) \tag{9}$$

$$b_4(\boldsymbol{r}) = e^{i\varphi}a_4(\boldsymbol{r}) \tag{10}$$

$$b_5(\boldsymbol{r}) = e^{i\varphi}a_5(\boldsymbol{r}+\boldsymbol{\alpha_2}) \tag{11}$$

$$b_6(\boldsymbol{r}) = e^{i\varphi}a_6(\boldsymbol{r}+\boldsymbol{\alpha_1}) \tag{12}$$

By looking for Bloch eigenstates, we obtain

$$|a(\boldsymbol{k})\rangle = e^{-i\varphi}\Lambda(\boldsymbol{k})|b(\boldsymbol{k})\rangle \tag{13}$$

where $\Lambda(\boldsymbol{k}) = \text{diag}\left(e^{i\boldsymbol{k}\cdot\boldsymbol{\alpha_2}}, e^{i\boldsymbol{k}\cdot\boldsymbol{\alpha_1}}, 1, 1, e^{-i\boldsymbol{k}\cdot\boldsymbol{\alpha_2}}, e^{-i\boldsymbol{k}\cdot\boldsymbol{\alpha_1}}\right)$ is a unitary matrix. Combining Equations (6) and (13), we obtain the eigenequation in momentum space formed by $S(\boldsymbol{k})$ as

$$S(\boldsymbol{k})|b(\boldsymbol{k})\rangle = e^{-i\varphi(\boldsymbol{k})}|b(\boldsymbol{k})\rangle \tag{14}$$

where $S(\boldsymbol{k}) = \Lambda^{-1}(\boldsymbol{k})S_{\text{unit cell}}$ is unitary, and $\varphi(\boldsymbol{k})$ is a real-valued phase defined modulo $[2\pi]$. The values of $\varphi(\boldsymbol{k})$ as a function of $\boldsymbol{k}$ define the phase band structure, which is similar to that of Floquet lattices where the quasi-energy plays the role of the phase-delay. Equation (14) defines the Bloch eigenproblem of our circulator network and consequently its topology.

Such unitary systems were topologically characterized by a homotopy invariant defined in each gap, W_ψ, that directly counts the net number of chiral edge states in a given gap,[34] which could be classified as unitary topology.

It is noted that the non-reciprocal scattering network was formally analogous to a rigorously oriented Kagome graph, described by a unitary matrix $S(\boldsymbol{k})$,[48] which could be mapped onto the Floquet (unitary) eigenproblem of a periodically-driven lattice, with the angle variable φ taking the role of the quasi-energy. Therefore, both advantages of non-reciprocity, and the potentially richer topological physics of Floquet (unitary) systems were truly beneficial. The topology of unitaries, such as evolution operators or the scattering matrix, were better described by the homotopy group $\pi_3(U(N)) = Z$, whose elements were the topological numbers

$$W_\psi(\varphi) = (24\pi^2)^{-1}\int \text{tr}(V_\varphi^{-1}\text{d}V_\varphi)^3 \quad \in \mathbb{Z} \tag{15}$$

The power 3 must be understood in the language of differential forms, and the integral runs over a 3-torus, span by the momentum and time t (over a time period T). Time was not explicit in scattering networks. However, the cyclicity of the network made possible a direct mapping with a Floquet (i.e. T-periodic in time) evolution operator $U(t, \boldsymbol{k})$, such that an interpolation parameter that formally played the role of time, could be introduced. Finally, the operator V_ψ was a periodized (in time) evolution operator. For Floquet systems, it reads as

$$V_\psi(t, \boldsymbol{k}) = U(t, \boldsymbol{k})e^{itH_{\text{eff}}(\boldsymbol{k})} \tag{16}$$

with

$$H_{\text{eff}}(\boldsymbol{k}) = \frac{i}{T}ln_{-\psi}U(t=T, \boldsymbol{k}) \tag{17}$$

where $-\psi$ denotes the branch-cut of the logarithm. The procedure to define such an operator V_ψ and thus the invariant W_ψ for discrete-time evolutions, (i.e. when the dynamics was given by a succession of scattering events and where time therefore does not appear explicitly), like in the model, was developed in a previous detailed study[48] (in particular in sections V. A. and V. B.). Importantly, the branch-cut ψ must be chosen in a spectral gap of $U(T, \boldsymbol{k})$, or $S(\boldsymbol{k})$ in the case. For this reason, W_ψ was said to be a gap invariant, and indeed directly gives the number of chiral edge states in a given quasi-energy gap φ. In contrast, Chern numbers were band invariants. They are inferred from $H_{\text{eff}}(\boldsymbol{k}) = \frac{i}{T}ln_{-\psi}U(t=T, \boldsymbol{k})$ and thus cannot capture the full unitary evolution. Finally, the details for the calculation of the invariants W_ψ in oriented Kagomé graphs could be found in Delplace et al.[48] Their values for the band structures of Figure 1b ($\theta = 0°$) are 1,1,1,1,1,1 in the anomalous case.

For the calculation of Chern number, the advantage of the typical Wilson–loop method was taken, and the Chern number is given as $C = \frac{1}{2\pi}\int d\theta_{k_y}$, where θ_{k_y} is the Berry phase defined as $\theta_{k_y} = \int dk_x \Lambda^{(x)}_{n,k}$ and $\Lambda^{(x)}_{n,k}$ is the Berry connection. The calculated Chern number for Figure 1b ($\theta = 0°$) are 0,0,0,0,0,0. Along with non-zero gap invariants for each band, the existence of anomalous phase with vanishing Chern number while maintaining edge states in every bandgap was confirmed.

Tunable unitary scatterers with controllable reflection strength θ could be introduced to the scattering network, in order to modulate the topological gap in the reconfigurable region, potentially modifying its topology. They play a similar role of impacting the topology through reflection (see Supporting Information) but without having to modify the circulators. The 2-by-2 unitary scattering matrix of the additional scatterers is defined as:

$$S_{scatter}(\theta) = \begin{pmatrix} i\sin\theta & \cos\theta \\ \cos\theta & i\sin\theta \end{pmatrix} \tag{18}$$

Two extreme cases are like on/off state of TL: when $\theta = 0°$, we have full transmission without reflection, and when $\theta = 90°$, we have full reflection instead.

These scatterers contribute to an additional unitary matrix in each unit cell as

$$S_{TL} = \begin{pmatrix} \cos\theta & & & & i\sin\theta & \\ & \cos\theta & & & & i\sin\theta \\ & & \cos\theta & i\sin\theta & & \\ & & i\sin\theta & \cos\theta & & \\ i\sin\theta & & & & \cos\theta & \\ & i\sin\theta & & & & \cos\theta \end{pmatrix} \tag{19}$$

Then the modified band structure reads

$$S(\boldsymbol{k}) = \Lambda_a^{-1}(\boldsymbol{k})S_{TL}\Lambda_c(\boldsymbol{k})S_{\text{unit cell}} \tag{20}$$

where $\Lambda_a(\boldsymbol{k}) = \text{diag}\left(\boldsymbol{I_4}, e^{i\boldsymbol{k}\cdot\boldsymbol{\alpha_2}}, e^{i\boldsymbol{k}\cdot\boldsymbol{\alpha_1}}\right)$, $\Lambda_c(\boldsymbol{k}) = \text{diag}\left(e^{i\boldsymbol{k}\cdot\boldsymbol{\alpha_2}}, e^{i\boldsymbol{k}\cdot\boldsymbol{\alpha_1}}, \boldsymbol{I_4}\right)$. The scattering strength θ impact the topology through controllable reflection on the transmission line as given in Equation (16) and Equation ((17)) in the Experimental Section, which tailors the Bloch eigenproblem by connecting $S(\boldsymbol{k})$ to depend on θ. The reflection and transmission coefficients on the bi-directional transmission line is $\sin\theta$ and $\cos\theta$, respectively. When $\theta = 0°$, the transmission line was full transmission without reflection, and the matrix in Equation (16) was an identity matrix which play no impact on the final $S(\boldsymbol{k})$. While $\theta \neq 0°$, transmission was suppressed with non-zero reflection, therefore off-diagonal terms in Equation (16) becoming prominent. This will tailor the overall performance of the band structure and thus topology derived from eigenproblem based on $S(\boldsymbol{k})$. This non-zero reflection on transmission line adds reflection in the unit

cell, which was unfavourable for anomalous topological insulators that required low reflection.[34,37] When large enough, the insulator will undergo topological phase transition from anomalous to Chern phase.[37]

For circulator networks with unobstructed transmission lines, the scattering strength vanishes ($\theta = 0°$), yielding

$$S_{scatter}(\theta = 0°) = \begin{pmatrix} 0 & 1 \\ 1 & 0 \end{pmatrix} \quad (21)$$

In this special case, there existed a chiral symmetry or sublattice symmetry that implied a π −phase translation symmetric band diagram with $\varphi(\boldsymbol{k}) = \varphi(\boldsymbol{k}) + \pi$ (see Supporting Information). Introducing scatterers with $\theta \neq 0°$ will break such chiral symmetry, therefore leading to the asymmetric band structures reported in the main text.

The band topology of circulators was analyzed at a constant frequency, which means that moving along the vertical axis φ in these $(k - \varphi)$ diagrams does not imply changing the frequency, but it means scaling up the length of the network links. For group velocity of such edge states, one needs to switch to the usual $(k - \omega)$ band diagram and look at the slope of the bands, as usual.[49] This can be done by taking into account the dispersion of the transmission lines and of the circulators (through Equation 6 in Supporting Information for example).

Experimental Set-Up: The non-reciprocal networks were designed and fabricated on 0.762 mm thick Rogers RT/duroid 4350 substrate. Each circulator node was a surface mount microwave circulator connected by microstrips. The circulator was designed from a Y-shaped strip line on a printed circuit board. The three ports were placed 120° apart from each other such that they were iso-spaced. The printed circuit board was sandwiched between two pieces of ferrite. Without magnetic fields, the Y-junction strip line supported two degenerate modes at ω_0: right and left-handed. To bias it, two magnets were fixed outside, providing the required magnetic field of 50 kA m^{-1} = 628 Oe, normal to the printed circuit board and polarizing the ferrite, therefore lifting the initial degeneracy, with chiral modes at ω_+ and ω_-. The voltage-tuned scatterer was realized by varactor-integrated split ring resonators. The varactor SMV1405 had voltage-controlled capacitance from 2.67 pF at 0 V to 0.63 pF at 30 V. Positive DC bias voltage was applied on the varactor and, to avoid the interference of DC components on the microwave network, low-pass filers were integrated in each resonator.

Supporting Information

Supporting Information is available from the Wiley Online Library or from the author.

Acknowledgements

This work was supported by the Swiss State Secretariat for Education, Research and Innovation (SERI) under contract number MB22.00028. The authors acknowledge useful discussions with Dr Pierre Delplace about the results of this study.

Open access funding provided by Ecole Polytechnique Federale de Lausanne.

Conflict of Interest

The authors declare no conflict of interest.

Data Availability Statement

The data that support the findings of this study are available from the corresponding author upon reasonable request.

Keywords

anomalous phase, edge states, metamaterials, nonreciprocity, reconfigurable, robustness, unitary topology

Received: February 1, 2024
Revised: March 28, 2024
Published online:

[1] Y. Zeng, U. Chattopadhyay, B. Zhu, B. Qiang, J. Li, Y. Jin, L. Li, A. G. Davies, E. H. Linfield, B. Zhang, Y. Chong, Q. J. Wang, *Nature* **2020**, *578*, 246.
[2] Y. Kang, X. Ni, X. Cheng, A. B. Khanikaev, A. Z. Genack, *Nat. Commun.* **2018**, *9*, 3029.
[3] Y. Yang, Z. Yang, B. Zhang, *J. Appl. Phys.* **2018**, *123*, 091713.
[4] S. Jia, S.-Y. Xu, M. Z. Hasan, *Nat. Mater.* **2016**, *15*, 1140.
[5] B. Yan, C. Felser, *Annu. Rev. Condens. Matter Phys.* **2017**, *8*, 337.
[6] P. Hosur, X. Qi, *C. R. Phys.* **2013**, *14*, 857.
[7] A. A. Burkov, L. Balents, *Phys. Rev. Lett.* **2011**, *107*, 127205.
[8] H. Xue, Y. Yang, F. Gao, Y. Chong, B. Zhang, *Nat. Mater.* **2019**, *18*, 108.
[9] J. Liu, T. H. Hsieh, P. Wei, W. Duan, J. Moodera, L. Fu, *Nat. Mater.* **2014**, *13*, 178.
[10] X. Ni, K. Chen, M. Weiner, D. J. Apigo, C. Prodan, A. Alú, E. Prodan, A. B. Khanikaev, *Commun. Phys.* **2019**, *2*, 1.
[11] F. D. M. Haldane, *Phys. Rev. Lett.* **1988**, *61*, 2015.
[12] Y. Hatsugai, *Phys. Rev. Lett.* **1993**, *71*, 3697.
[13] M. C. Rechtsman, J. M. Zeuner, Y. Plotnik, Y. Lumer, D. Podolsky, F. Dreisow, S. Nolte, M. Segev, A. Szameit, *Nature* **2013**, *496*, 196.
[14] J. Cayssol, B. Dóra, F. Simon, R. Moessner, *Phys. Status Solidi* **2013**, *7*, 101.
[15] M. Z. Hasan, C. L. Kane, *Rev. Mod. Phys.* **2010**, *82*, 3045.
[16] X.-L. Qi, S.-C. Zhang, *Rev. Mod. Phys.* **2011**, *83*, 1057.
[17] J. Costantine, Y. Tawk, S. E. Barbin, C. G. Christodoulou, *Proc. IEEE* **2015**, *103*, 424.
[18] C.-H. Lu, A. Cecconello, I. Willner, *J. Am. Chem. Soc.* **2016**, *138*, 5172.
[19] Q. He, S. Sun, L. Zhou, *Research* **2019**, *2019*, 1849272.
[20] M. D. Renzo, M. Debbah, D.-T. Phan-Huy, A. Zappone, M.-S. Alouini, C. Yuen, V. Sciancalepore, G. C. Alexandropoulos, J. Hoydis, H. Gacanin, J. d. Rosny, A. Bounceur, G. Lerosey, M. Fink, *EURASIP Journal on Wireless Communications and Network* **2019**, *2019*, 129.
[21] M. Nance Hall, K.-T. Foerster, S. Schmid, R. Durairajan, *Opt. Switch.Netw.* **2021**, *41*, 100621.
[22] M. I. Shalaev, S. Desnavi, W. Walasik, N. M. Litchinitser, *New J. Phys.* **2018**, *20*, 023040.
[23] X. Cheng, C. Jouvaud, X. Ni, S. H. Mousavi, A. Z. Genack, A. B. Khanikaev, *Nat. Mater.* **2016**, *15*, 542.
[24] A. Darabi, M. J. Leamy, *J.Acous. Soc. Am.* **2019**, *146*, 773.
[25] T. Cao, L. Fang, Y. Cao, N. Li, Z. Fan, Z. Tao, *Sci. Bull.* **2019**, *64*, 814.
[26] N. Gao, S. Qu, L. Si, J. Wang, W. Chen, *Appl. Phys. Lett.* **2021**, *118*, 063502.
[27] Y. Wang, Y. Dong, S. Zhai, C. Ding, C. Luo, X. Zhao, *Phys. Rev. B* **2020**, *102*, 174107.
[28] X. Ni, M. Weiner, A. Alú, A. B. Khanikaev, *Nat. Mater.* **2019**, *18*, 113.
[29] T.-W. Liu, F. Semperlotti, *Phys. Rev. Appl.* **2018**, *9*, 014001.
[30] H. Li, C. Ouyang, J. Ma, S. Liu, Y. Liu, Q. Xu, Y. Li, Z. Tian, J. Gu, J. Han, W. Zhang, *IEEE Phot. J.* **2022**, *14*, 1.
[31] M. McGinley, N. R. Cooper, *Nat. Phys.* **2020**, *16*, 1181.
[32] C. A. Rosiek, G. Arregui, A. Vladimirova, M. Albrechtsen, B. Vosoughi Lahijani, R. E. Christiansen, S. Stobbe, *Nat. Photonics* **2023**, *17*, 386.
[33] M. C. Rechtsman, *Nat. Photonics* **2023**, *17*, 383.

[34] M. S. Rudner, N. H. Lindner, E. Berg, M. Levin, *Phys. Rev. X* **2013**, *3*, 031005.
[35] S. Afzal, T. J. Zimmerling, Y. Ren, D. Perron, V. Van, *Phys. Rev. Lett.* **2020**, *124*, 253601.
[36] M. Pasek, Y. D. Chong, *Phys. Rev. B* **2014**, *89*, 075113.
[37] Z. Zhang, P. Delplace, R. Fleury, *Nature* **2021**, *598*, 293.
[38] Z. Zhang, P. Delplace, R. Fleury, *Sci. Adv.* **2023**, *9*, eadg3186.
[39] Y. Zhang, Q. Du, C. Wang, T. Fakhrul, S. Liu, L. Deng, D. Huang, P. Pintus, J. Bowers, C. A. Ross, J. Hu, L. Bi, *Optica* **2019**, *6*, 473.
[40] Z. Wang, S. Fan, *Appl. Phys. B* **2005**, *81*, 369.
[41] D. L. Sounas, C. Caloz, A. Alú, *Nat. Commun.* **2013**, *4*, 2407.
[42] L. Bi, J. Hu, P. Jiang, D. H. Kim, G. F. Dionne, L. C. Kimerling, C. A. Ross, *Nat. Photonics* **2011**, *5*, 758.
[43] M. Samizadeh Nikoo, E. Matioli, *Nature* **2023**, *614*, 451.
[44] B. Lian, X.-Q. Sun, A. Vaezi, X.-L. Qi, S.-C. Zhang, *Proc. Nat. Acad. Sci.* **2018**, *115*, 10938.
[45] A. Stern, N. H. Lindner, *Science* **2013**, *339*, 1179.
[46] R. Fleury, D. L. Sounas, C. F. Sieck, M. R. Haberman, A. Alú, *Science* **2014**, *343*, 516.
[47] A. B. Khanikaev, R. Fleury, S. H. Mousavi, A. Alú, *Nat. Commun.* **2015**, *6*, 8260.
[48] P. Delplace, M. Fruchart, C. Tauber, *Phys. Rev. B* **2017**, *95*, 205413.
[49] R. Fleury, A. B. Khanikaev, A. Alú, *Nat. Commun.* **2016**, *7*, 11744.